

Cite this: *Dalton Trans.*, 2020, **49**, 388

# An organic chromophore -modified samarium-containing polyoxometalate: excitation-dependent color tunable behavior from the organic chromophores to the lanthanide ion†

Hechen Wu, <sup>a,b</sup> Bing Yan,<sup>a</sup> Rongchang Liang,<sup>a</sup> Vikram Singh,<sup>a</sup> Pengtao Ma, <sup>\*a</sup> Jingping Wang <sup>a</sup> and Jingyang Niu <sup>\*a</sup>

Here, an organic–inorganic hybrid lanthanide-based polyoxometalate (Ln-POM)  $[\text{N}(\text{CH}_3)_4]_3\text{K}_2\text{Sm}(\text{C}_7\text{H}_5\text{O}_2)(\text{H}_2\text{O})_2(\alpha\text{-PW}_{11}\text{O}_{39})\cdot 11\text{H}_2\text{O}$  (**1**) was successfully synthesized and characterized well by several physico-chemical techniques. In the polyanion of **1**, the benzoic acid ligand directly binds a  $\text{Sm}^{3+}$  ion for the formation of an organic–inorganic hybrid polyanion. This organic–inorganic hybrid structure can effectively sensitize the emissions of the  $\text{Sm}^{3+}$  ion, which was confirmed by the photoluminescence and time-resolved emission spectroscopy of **1**. The photoluminescence study demonstrates that the  $\text{Sm}^{3+}$  ion possesses a relatively high-symmetry coordination geometry, which is consistent with the structural analysis of  $\text{Sm}^{3+}$  in **1**. Furthermore, the polyanion of **1** can form a 3D 4,8-topology framework through the linkage of K1 and K2 ions. In addition, the photoluminescence properties of **1** have been explored, revealing that **1** shows reversible color-tunable photoluminescence based on the excitation from 260 nm to 350 nm, and emitting colors from blue to pink.

Received 14th September 2019,  
Accepted 25th November 2019

DOI: 10.1039/c9dt03681d

rsc.li/dalton

## Introduction

Polyoxometalates (POMs) represent a family of anionic metal oxide clusters, which are composed of a series of metal oxides  $\{\text{MO}_x\}$  ( $\text{M} = \text{V}^{5+}, \text{Nb}^{5+}, \text{Ta}^{5+}, \text{Mo}^{6+}, \text{W}^{6+}$ ) in their highest oxidation state fused together through the edge-, corner- or face-shared methods.<sup>1</sup> Over the past decades, the relative investigation and applications of POM chemistry have seen huge developments in leaps and bounds, not only in the novel and varied structures of reported complexes, but also in a lot of interesting properties including catalysis, magnetism, optics, and medicinal chemistry.<sup>2</sup> The lanthanide (Ln)-based POMs (Ln-POMs), as one of the most important branches in POM chemistry, have attracted more and more attention since the first discovery of Ln-POMs in 1971.<sup>3</sup> Till now, Ln-POMs have

been studied and applied in several areas, such as photoluminescent materials, sensors, magnetic materials, organo-catalysts, photochromic materials and so on.<sup>4</sup> With regard to the photoluminescence properties of Ln-POMs, the POM component can be seen as an appropriate light-harvesting candidate to sensitize the emissions of the  $\text{Ln}^{3+}$  center through an intramolecular energy transfer from the  $\text{O} \rightarrow \text{M}$  photo-excitation state to the ligand to metal charge transfer (LMCT) state within Ln-POMs matrices.<sup>5</sup> The research regarding the photoluminescence and photophysical behavior of Ln-POMs, including their inherent emissions, luminescence lifetime, emitting color and energy transfer mechanism, has been widely recognized.<sup>6</sup> In addition, further investigations on the photoluminescence of Ln-POM derivatives, like the color-tuning property, which can be generally achieved by adjusting the molar ratio of  $\text{Ln}^{3+}$  ions or altering the excitation wavelength, are urgently needed.<sup>7</sup>

Early works regarding the color-tuning properties of Ln-POMs were discussed by Wu, Zhou and Van Deun in recent years, and our group also made several contributions in this field. In detail, Wu and co-workers first reported several emissive Ln-POMs  $\{[\text{Ln}_2(\text{DMF})_8(\text{H}_2\text{O})_6][\text{ZnW}_{12}\text{O}_{40}]\cdot 4\text{DMF}$  ( $\text{Ln}^{3+} = \text{La}^{3+}, \text{Eu}^{3+}, \text{and Tb}^{3+}$ ), which exhibited interesting color-tunable and white light-emitting properties through changing the molar ratio of  $\text{Eu} : \text{Tb}$  in 2012.<sup>8</sup> In 2017, Zhou's group com-

<sup>a</sup>Henan Key Laboratory of Polyoxometalate Chemistry, College of Chemistry and Chemical Engineering, Henan University, Kaifeng, Henan 475004, P. R. China.  
E-mail: mpt@henu.edu.cn, jyniu@henu.edu.cn; Fax: (+86)-371-23886876

<sup>b</sup>Department of Chemistry, Fudan University, Shanghai 200433, China

†Electronic supplementary information (ESI) available: PXRD, FTIR spectroscopy, TGA curve, coordination environment of K1 and K2 ions, photoluminescence excitation and emission maps (EEMs) of **1**. CCDC 1940262. For ESI and crystallographic data in CIF or other electronic format see DOI: 10.1039/c9dt03681d

municated a series of isostructural compounds  $\text{Na}(\text{HL})(\text{CH}_3\text{COO})\text{Eu}_m\text{Tb}_n\text{La}_{1-m-n}(\text{AlMo}_6(\text{OH})_6\text{O}_{18})\cdot(\text{H}_2\text{O})_6\cdot 10\text{H}_2\text{O}$  ( $\text{L} = \text{nicotinate}$ ) based on Anderson-type polyanions  $[\text{AlMo}_6(\text{OH})_6\text{O}_{18}]^{3-}$ , which displayed tunable luminescence colors, and the white light-emitting behavior could be realized by adjusting the molar ratio of  $\text{Eu} : \text{Tb} : \text{La}$ .<sup>9a</sup> Subsequently, Zhou and co-workers obtained another white light-emitting thin film based on a pure inorganic Ln-POM,  $\text{Na}_9\text{Eu}_m\text{Tb}_n\text{Ce}_{1-m-n}\text{W}_{10}\text{O}_{36}$ , in 2018.<sup>9b</sup> In 2019, Kaczmarek *et al.* obtained a series of  $\text{Eu}^{3+}$ -doped  $\text{Lu}^{3+}$ -octamolybdates, and investigations of their luminescence revealed that they exhibit emission ranging from blue to strong red.<sup>10</sup> In addition, our group reported a helical chain-like organic-inorganic hybrid arsenotungstate  $\text{Na}_4\text{H}_8[\{\text{Pr}(\text{H}_2\text{O})_2\}_2\{\text{As}_2\text{W}_{19}\text{O}_{68}\}\{\text{WO}_2(\text{mal})\}_2]\cdot 24\text{H}_2\text{O}$  with color-tunable photoluminescence in 2018.<sup>11a</sup> In the same year, we reported another  $\text{Tm}^{3+}/\text{Dy}^{3+}$  co-doped POM  $[\text{N}(\text{CH}_3)_4]_6\text{K}_3\text{H}_7[\text{Dy}_x\text{Tm}_{1-x}(\text{C}_4\text{H}_2\text{O}_6)(\alpha\text{-PW}_{11}\text{O}_{39})]_2\cdot 27\text{H}_2\text{O}$ , which exhibits color-tunable luminescence, emitting in the range from blue to white to yellow.<sup>11b</sup> This year, we have successfully synthesized multicenter-Ln polyoxometalate derivatives  $[\text{N}(\text{CH}_3)_4]_3\text{K}_2\text{Eu}_x\text{Tb}_y\text{Tm}_{1-x-y}(\text{C}_7\text{H}_5\text{O}_2)(\text{H}_2\text{O})_2(\alpha\text{-PW}_{11}\text{O}_{39})\cdot 11\text{H}_2\text{O}$ . The study indicates that the white light-emitting behavior could be achieved by adjusting the molar ratio of  $\text{Eu}^{3+}/\text{Tb}^{3+}/\text{Tm}^{3+}$ .<sup>11c</sup> In the previous research, it can be found that most of the reported color-tuning Ln-POMs are achieved through adjusting the type and proportion of the  $\text{Ln}^{3+}$  ion component within the same matrix. One case reported by our group realized the color-tuning behavior by just changing the excitation wavelength. As we know, it is easy to achieve the color-tuning behaviors of complexes through changing the type and proportion of the  $\text{Ln}^{3+}$  ion, yet this method may result in a considerable waste of rare earth resources. Furthermore, it is difficult to accurately detect the content in the doped complexes. Therefore, an economical strategy to achieve color-tuning behavior is to alter the excitation wavelength in a single component.

In this work, we successfully synthesized an organic-inorganic hybrid Ln-POM  $[\text{N}(\text{CH}_3)_4]_3\text{K}_2\text{Sm}(\text{C}_7\text{H}_5\text{O}_2)(\text{H}_2\text{O})_2(\alpha\text{-PW}_{11}\text{O}_{39})\cdot 11\text{H}_2\text{O}$  (**1**), which was characterized by single crystal X-ray diffraction analysis, elemental analyses, powder X-ray diffraction (PXRD) (Fig. S1†), Fourier transform infrared (FTIR) spectroscopy (Fig. S2†) and thermogravimetric analyses (TGA) (Fig. S3†). The structural study shows that the polyanion of **1** could construct a 3D framework through the connection of K1 and K2 ions. Furthermore, the photoluminescence and energy transfer mechanism within **1** have been investigated by various physicochemical techniques. The results reveal that **1** can display color-tunable emission from blue to pink upon changing the excitation wavelength. Differently, the emitting color can be tuned from green to yellow as a result of the variation in emission either from the POM component or  $\text{Pr}^{3+}$  ion, as reported in our previous work.<sup>11a</sup> Here, the emitting color could be tuned through the variation of emission intensity of the organic chromophore group (blue) and the  $\text{Sm}^{3+}$  emitting center (red) under different excitation wavelengths.

## Results and discussion

### Crystal structure

Compound **1** was synthesized by the reaction of  $\text{K}_{14}[\text{P}_2\text{W}_{19}\text{O}_{69}(\text{H}_2\text{O})]\cdot 24\text{H}_2\text{O}$  precursor,  $\text{SmCl}_3\cdot 6\text{H}_2\text{O}$  and benzoic acid ligand in appropriate proportions using a conventional aqueous solution method. In the synthesis process, the  $\text{K}_{14}[\text{P}_2\text{W}_{19}\text{O}_{69}(\text{H}_2\text{O})]\cdot 24\text{H}_2\text{O}$  precursor was easily decomposed into several POM pieces in an aqueous solution, such as a  $[\alpha\text{-PW}_{11}\text{O}_{39}]^{7-}$  fragment, which can construct multifarious POM derivatives. In this system, the  $\text{K}_{14}[\text{P}_2\text{W}_{19}\text{O}_{69}(\text{H}_2\text{O})]\cdot 24\text{H}_2\text{O}$  precursor reacts with the  $\text{Sm}^{3+}$  ion and benzoic acid ligand under an optimum pH value of 4.5 in aqueous solution, leading to the crystallization of **1**. The structural analysis reveals that **1** crystallizes in the  $P\bar{1}$  space group of the triclinic system, which contains a mono-lacunary Keggin-type  $[\text{Sm}(\text{C}_7\text{H}_5\text{O}_2)(\text{H}_2\text{O})_2(\alpha\text{-PW}_{11}\text{O}_{39})]^{5-}$  polyanion, three  $[\text{N}(\text{CH}_3)_4]^+$  counter-cations, two  $\text{K}^+$  ions and eleven lattice water molecules.

In the polyanion of **1**, the  $\text{Sm}^{3+}$  ion was embedded into the vacant site of the mono-lacunary  $[\alpha\text{-PW}_{11}\text{O}_{39}]^{7-}$  unit through the formation of four  $\text{Sm}-\text{O}$  (O13, O16, O19, O30) bonds with a length of 2.326(9)–2.393(9) Å, and one benzoic acid ligand simultaneously coordinates to the  $\text{Sm}^{3+}$  ion through the two carboxylate oxygen atoms of the benzoic acid ligand with the distance of the  $\text{Sm}-\text{O}$  (O40, O41) bond ranging from 2.502(10) Å to 2.526(10) Å. Furthermore, another two water oxygen atoms (O1 W, O2 W) also participate in the coordination environment of the  $\text{Sm}^{3+}$  ion, and the length of the  $\text{Sm}-\text{O}$  bond is in the range of 2.483(11)–2.484(13) Å (Fig. 1a, Table S1†). In the coordination environment of the  $\text{Sm}^{3+}$  center, the  $\text{Sm}^{3+}$  ion adopts an eight-coordinate distorted square antiprismatic configuration. The two bottom planes for the  $\text{Sm}^{3+}$  coordination geometry are achieved by oxygen atoms O13, O16, O19, O30 and O40, O41, O1 W, O2 W with the average deviations of least-squares planes of 0.006 and 0.013 Å (Fig. 1b). In addition, the length of the  $\text{W}-\text{O}$  bond ranges from 1.697(11) Å to 2.524(9) Å with an average bond of 1.968(9) Å, and the angles of the  $\text{O}-\text{W}-\text{O}$  bond are in the range of 70.3(3)–172.8(4)° with an average angle of 103.5(4)° (Table S2†). All the above mentioned bond lengths and angles of **1** are consistent with that of the reported literature.<sup>6a</sup>

The polyanion of **1** can further form a 3D framework through the connection of K1 and K2 ions (Fig. 1c). From a topological point of view, if the  $[\text{Sm}(\text{C}_7\text{H}_5\text{O}_2)(\text{H}_2\text{O})_2(\alpha\text{-PW}_{11}\text{O}_{39})]^{5-}$  polyanions are seen as the linked nodes with the K1 and K2 cations as bridges, the structure exhibits a 3D 4,8-topology framework (Fig. 2). In the formation process of a 3D framework, the K1 ion adopts a four-coordinated configuration, which is achieved by four oxygen atoms (O4 W, O6, O30, O41) with K1–O bond lengths of 2.686(14)–2.797(9) Å (Fig. S4, Table S1†). Differently, the K2 ion was surrounded by five oxygen atoms (O8 W, O9 W, O3, O7, O8), and the lengths of the K2–O bonds are in the region of 2.717(11)–2.793(11) Å in **1** (Fig. S5, Table S1†).

### Photoluminescence properties

As we know, the luminescence of the  $\text{Ln}^{3+}$  emitting center is limited by the small molar absorption coefficients due to the

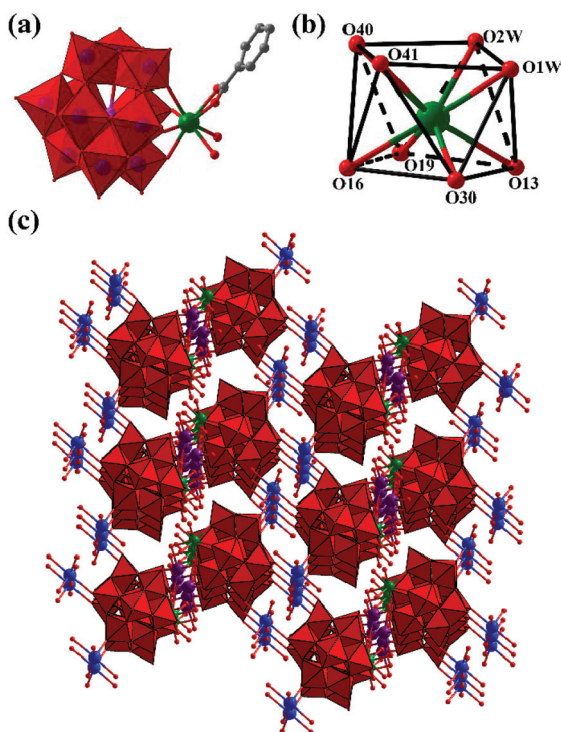


**Fig. 1** (a) Polyhedral/ball-and-stick representation of the polyanion in **1**; (b) the coordination environment of the Sm center; (c) polyhedral/ball-and-stick representation of the 3D framework of polyanion **1**, benzoic acid ligands were omitted for clarity (color code:  $\text{WO}_6$ , red; P, pink; Sm, green; O, red; C, gray; K1, violet; K2, blue).

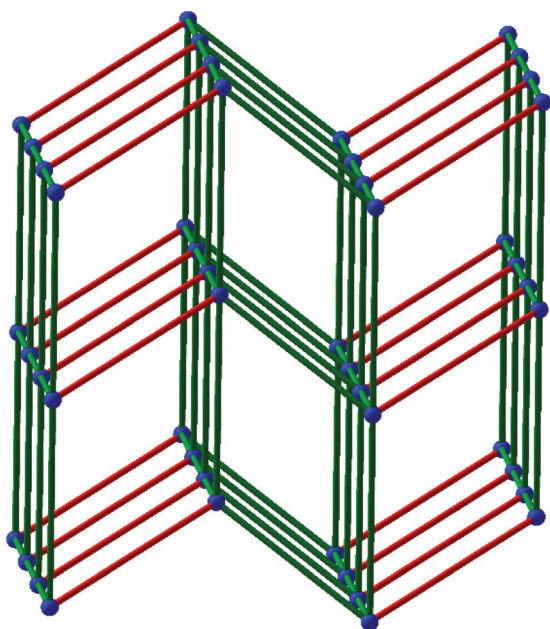


**Fig. 2** The 3D topological framework of **1**. Blue balls represent the polyanion  $[\text{Sm}(\text{C}_7\text{H}_5\text{O}_2)(\text{H}_2\text{O})_2(\alpha\text{-PW}_{11}\text{O}_{39})]^{5-}$ ; red lines represent K1 ions; green lines represent K2 ions.

electric-dipole-forbidden nature of the  $f-f$  transitions; hence, some sensitizers were required to overcome the bottleneck and sensitize the emissions of the  $\text{Ln}^{3+}$  ion.<sup>12</sup> According to the reported literature, the photoluminescence of Ln-POMs and their derivatives have been systematically investigated.<sup>6a,13</sup> POM fragments can be considered as a type of light-harvesting sensitizer to harvest energy, which can subsequently be transferred to the  $\text{Ln}^{3+}$  ion. First, the POM was excited from the  $^1\text{A}_{1g}$  ground state to the  $^1\text{T}_{1u}$  triplet state and returned to the  $^3\text{T}_{1u}$  triplet state through a fast nonradiative transition; second, the photoexcited  $^3\text{T}_{1u}$  triplet state can transfer energy and sensitize the emissions of the  $\text{Ln}^{3+}$  ion through an intramolecular energy transfer mechanism. However, the very low energy-transfer efficiency from the POM component to  $\text{Ln}^{3+}$  strongly limits the applications of Ln-POMs, and the reported quantum yield of the most intense Ln-POM was about 1%.<sup>13a</sup> Therefore, the organic chromophores were mainly introduced into the Ln-POM system for the sensitization of the  $\text{Ln}^{3+}$  ion. The sensitizing mechanism from the organic chromophores to  $\text{Ln}^{3+}$  has been explored: the organic chromophore was first excited from the ground state to a singlet state ( $\text{S}_1$ ) and then to a triplet state ( $\text{T}_1$ ) through an intersystem crossing process; then, the energy transfer from the triplet state ( $\text{T}_1$ ) can induce the sensitization of  $\text{Ln}^{3+}$  through a Dexter-type energy transfer mechanism.<sup>13b</sup> These explorations have proved that the organic chromophore ligands would provide a more efficient energy transfer approach for sensitizing the emissions of  $\text{Ln}^{3+}$  ions in the Ln-POMs derivatives. Recently, our group also confirmed that *p*-hydroxybenzoic ligand can sensitize the luminescence emission of a  $\text{Eu}^{3+}$  ion within organic-inorganic hybrid Ln-POMs.<sup>14</sup>

Herein, the solid-state photoluminescence of **1** was measured at room temperature. As shown in Fig. S6,<sup>†</sup> the excitation spectrum of **1** was recorded on the emission at 599 nm. The excitation spectrum displays a weak broad band from 250 nm to 350 nm, which can be attributed to the  $\pi-\pi^*$  transition of the organic benzoic acid ligand, and two sharp peaks at 365 and 377 nm, which are characteristic of direct excitation transitions of  $\text{Sm}^{3+}$ ,  $^6\text{H}_{5/2} \rightarrow ^4\text{L}_{15/2}$  and  $^6\text{H}_{5/2} \rightarrow ^6\text{P}_{7/2}$ . The presence of both weak and broad bands in the excitation spectrum demonstrates that the benzoic acid ligand can absorb energy and sensitize the luminescence emission of  $\text{Sm}^{3+}$ . In light of the excitation spectrum, the emission spectrum of **1** was recorded at the excitation wavelength of 310 nm at room temperature. Five emission peaks can be noticed at 435, 564, 599, 646 and 705 nm in the emission spectrum of **1** (Fig. 3). The broad emission centered at 435 nm was mainly assigned to the  $\pi^*-\pi$  transitions of the organic component in **1**, while a similar exploration has been recently reported by our group, which revealed the presence of a benzoic acid group in **1**.<sup>14</sup> To further explore the origin of the broad emission from 400 nm to 500 nm, the photoluminescence emission spectra of the benzoic acid ligand and  $\text{K}_{14}[\text{P}_2\text{W}_{19}\text{O}_{69}(\text{H}_2\text{O})]\cdot 24\text{H}_2\text{O}$  precursor were recorded at the excitation wavelength of 310 nm under the same conditions. As shown in Fig. S7,<sup>†</sup> the emission intensity of the benzoic acid ligand was much larger than that of

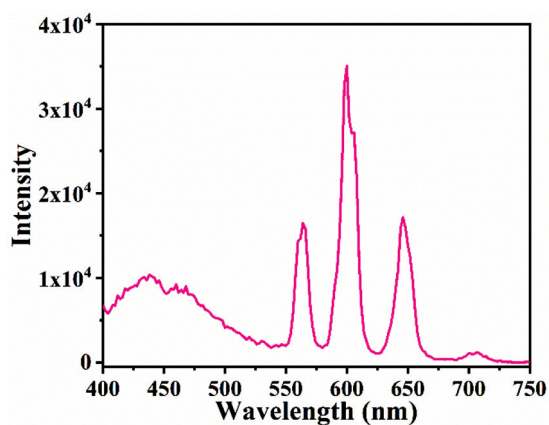


Fig. 3 The photoluminescence emission spectrum of **1** under excitation at 310 nm.

the  $K_{14}[P_2W_{19}O_{69}(H_2O)] \cdot 24H_2O$  precursor, which indicates that the broad emission centered at 435 nm originates mainly from the emission of the benzoic acid ligand. The other four peaks at 564, 599, 646 and 705 nm could be attributed to the characteristic  $^4G_{5/2} \rightarrow ^6H_{5/2}$ ,  $^4G_{5/2} \rightarrow ^6H_{7/2}$ ,  $^4G_{5/2} \rightarrow ^6H_{9/2}$ , and  $^4G_{5/2} \rightarrow ^6H_{11/2}$  transitions of  $Sm^{3+}$ . It is well-known that both magnetic-dipole and electric-dipole transitions exist together in the characteristic f-f transitions of  $Ln^{3+}$ . The four characteristic  $^4G_{5/2} \rightarrow ^6H_{5/2}$ ,  $^4G_{5/2} \rightarrow ^6H_{7/2}$ ,  $^4G_{5/2} \rightarrow ^6H_{9/2}$ , and  $^4G_{5/2} \rightarrow ^6H_{11/2}$  transitions of  $Sm^{3+}$  belong to the magnetic-dipole, magnetic-dipole, electric-dipole, and electric-dipole transitions, respectively.<sup>6a</sup> Generally, the magnetic-dipole transitions were insensitive to the coordination environment of the  $Sm^{3+}$  ion, whereas the electric-dipole transitions was very sensitive to the local environment. The low-symmetry coordination environment would facilitate the emission intensity of  $Ln^{3+}$ . Thus, the intensity ratio of  $^4G_{5/2} \rightarrow ^6H_{5/2}/^4G_{5/2} \rightarrow ^6H_{9/2}$  was always considered as an important indicator to estimate the symmetry of the coordination environment of the  $Sm^{3+}$  emitting center.<sup>15</sup> With regard to the photoluminescence of **1**, the intensity ratio of  $^4G_{5/2} \rightarrow ^6H_{5/2}/^4G_{5/2} \rightarrow ^6H_{9/2}$  was about 1:1, strongly proving that  $Sm^{3+}$  adopts a relatively high-symmetry coordination geometry. The results are in good agreement with the structural analysis of the  $Sm^{3+}$  ion within **1**.

### Energy transfer mechanism

The energy transfer dynamics of organic-inorganic hybrid Ln-POMs have been investigated by Francesconi, Boskovic and our group.<sup>13b,14,16</sup> Herein, time-resolved emission spectroscopy was used to study the energy transfer mechanism in **1**. As shown in Fig. 4, time-resolved emission spectroscopy of **1** was performed under an excitation of 310 nm at room temperature. An intriguing discovery revealed that the distinct features evolve from 38.0  $\mu s$  to 90.0  $\mu s$  during the time-resolved emission spectroscopy experiment. Upon excitation at 310 nm, an intense emission band around 435 nm appeared at 38.0  $\mu s$ , which corresponds to the  $\pi^*-\pi$  transition of the benzoic acid group in **1**. Subsequently, the emission features at 564, 599

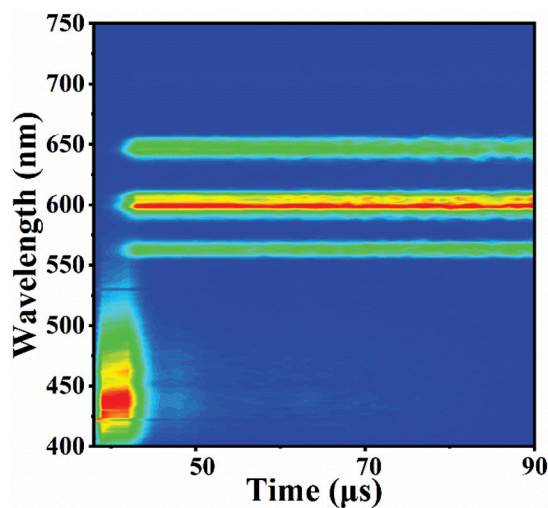


Fig. 4 The time resolved emission spectroscopy of **1** under excitation at 310 nm.

and 646 nm were initially discovered at 41.0  $\mu s$ , and the peaks can be assigned to the f-f transitions of the  $Sm^{3+}$  ion. Meanwhile, the intensity of the benzoic-centered emission at 435 nm generally declines, and it fades away until reaching 43.0  $\mu s$ . The characteristic emission intensity of  $Sm^{3+}$  gradually increases to the maximum value until 42.5  $\mu s$ . As the spectrum decays, the characteristic emission intensity of the  $Sm^{3+}$  ion remains dominant after 42.5  $\mu s$ . The time-resolved emission spectroscopy strongly suggested that the benzoic acid group can sensitize the luminescence emissions within **1**. The possible process of energy transfer is shown in Fig. 5 to explain the energy transfer pathway in **1** upon irradiation. In addition, the POM group can also be considered as an appropriate candidate to sensitize the emissions of the  $Ln^{3+}$  centers, which has

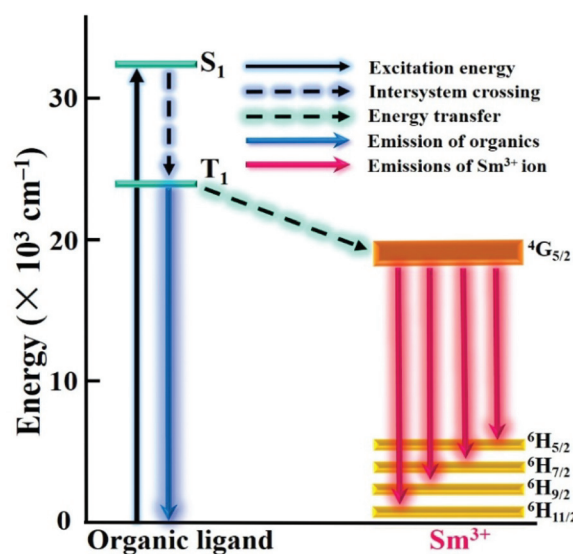


Fig. 5 The schematic energy level diagram and energy transfer (ET) process in **1**.

been widely investigated. Here, the POM fragments can also sensitize the emissions of  $\text{Sm}^{3+}$ ; hence a double antenna effect from both the POM and benzoate ligand may occur in this Sm-POM. However, a much lower energy-transfer efficiency may appear between the POM group and  $\text{Sm}^{3+}$  ion because of the weak emission of the POM fragment (Fig. S7†).

### Color-tunable photoluminescence properties

Interestingly, **1** may possess excitation wavelength dependent emission properties. As shown in Fig. 6, the 3D excitation-emission map (EEM) of **1** displays different photoluminescence emission signals under different excitation wavelengths from 260 nm to 350 nm. Notably, the broad emission centered at 435 nm was predominant when the excitation wavelength was 260 nm, while the emission intensity of  $\text{Sm}^{3+}$  also exhibits strong emission bands. Thus, the emission of **1** under excitation at 260 nm corresponds to a blue color in the CIE 1931 chromaticity chart. With the increase in the excitation wavelengths, the emission intensity around 435 nm generally weakens, whereas the emission intensity of the  $\text{Sm}^{3+}$  ion increases. Simultaneously, the CIE 1931 chromaticity coordinates vary from the blue area (0.257, 0.199) to the pink area (0.347, 0.258), and the correlated color temperature (CCT) varies from 247 341 K to 4249 K (Fig. 7, Table 1). Subsequently, the emission intensity around 435 nm generally increased as the excitation wavelength increased, and the emission color also changed from pink (0.347, 0.258) to blue (0.233, 0.156). In addition, the other 3D EEMs from different angles of view are shown in Fig. S8–10.† The comparison of the emission intensity of the benzoic acid ligand and  $\text{K}_{14}[\text{P}_2\text{W}_{19}\text{O}_{69}(\text{H}_2\text{O})]\cdot 24\text{H}_2\text{O}$  precursor indicates that the main origin of the blue emissions of the Sm-POM may be assigned to the emission of the organic ligands rather than the POM fragment. This interesting phenomenon reveals that the luminescence emission color of

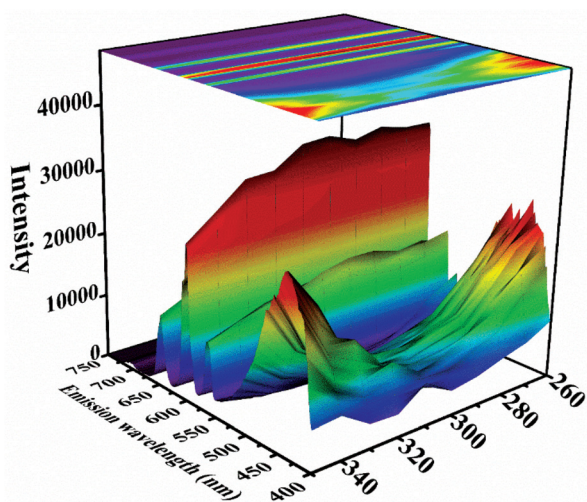


Fig. 6 The 3D color surface plots (bottom) and corresponding 2D diagrams (top) of photoluminescence excitation and emission maps (EEMs) of **1**. Note that the emission intensity increases as the color changes from blue to red.

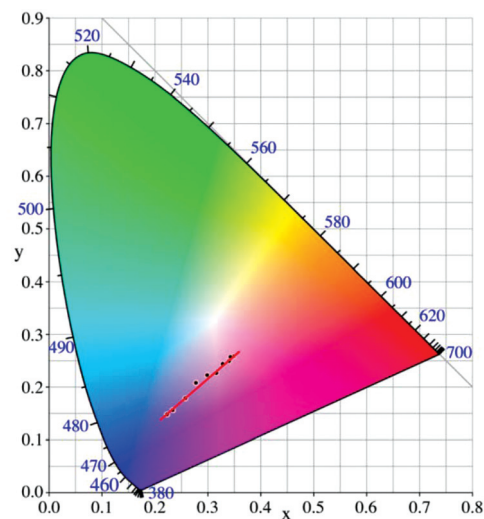


Fig. 7 The CIE 1931 chromaticity coordinates corresponding to the emission spectra of **1** based on the serial excitation wavelengths from 260 nm to 350 nm.

Table 1 CIE chromaticity coordinates, correlated color temperature (CCT) and emitting color of **1**

Excitation wavelength (nm)	(x, y)	CCT (K)	Emitting color
260	0.257, 0.199	247 341	Blue
270	0.277, 0.208	51 736	Blue
280	0.298, 0.222	15 501	Blue
290	0.327, 0.244	6131	Blue-pink
300	0.343, 0.257	4546	Pink
310	0.347, 0.258	4249	Pink
320	0.339, 0.250	4814	Pink
330	0.316, 0.227	8741	Blue-pink
340	0.278, 0.192	650 691	Blue
350	0.233, 0.156		Blue

**1** can be reversibly tuned from blue to pink by varying the excitation wavelength. This study makes it possible to achieve reversible emission color switching by simply changing the excitation wavelength rather than adjusting the doped ratio of  $\text{Ln}^{3+}$  ions within organic-inorganic hybrid Ln-POMs.

## Conclusion

In summary, an organic-inorganic hybrid Ln-POM  $[\text{N}(\text{CH}_3)_4]_3\text{K}_2\text{Sm}(\text{C}_7\text{H}_5\text{O}_2)(\text{H}_2\text{O})_2(\alpha\text{-PW}_{11}\text{O}_{39})\cdot 11\text{H}_2\text{O}$  (**1**) was successfully synthesized and characterized by single crystal X-ray diffraction analysis, elemental analyses, PXRD, FTIR spectroscopy and TGA analysis. The structural analyses indicated that the benzoic acid ligand directly coordinates to the  $\text{Sm}^{3+}$  ion in the polyanion of **1**, and the polyanion can further construct a 3D framework through the connection of K1 and K2 cations. The photoluminescence and time-resolved emission spectroscopy revealed that the organic benzoic group can sensitize the luminescence emissions of the  $\text{Sm}^{3+}$  ion within **1**. Furthermore, **1** may possess excitation wavelength dependent

emission based on the excitation from 260 nm to 350 nm, and the emitting color can be reversibly tuned from blue to pink. This investigation may provide a facile approach to achieve reversible emission color switching simply by altering the excitation wavelength instead of adjusting the doped ratio of  $\text{Ln}^{3+}$  ions.

## Experimental

### Material and physical measurements

All chemicals were commercially purchased and used without any further purification. The  $\text{K}_{14}[\text{P}_2\text{W}_{19}\text{O}_{69}(\text{H}_2\text{O})]\cdot 24\text{H}_2\text{O}$  precursor was synthesized according to literature and confirmed by FTIR spectroscopy.<sup>17</sup> C, H, and N elemental analyses were recorded on an Elementar Vario EL cube CHNS analyzer. PXRD was performed using an X-ray powder diffractometer (Bruker, D8 Advance) using  $\text{Cu K}\alpha$  radiation ( $\lambda = 1.5418 \text{ \AA}$ ) collected with the angular range ( $2\theta$ ) from  $5^\circ$  to  $45^\circ$  at room temperature. FTIR spectra (KBr disk) were collected on a Bruker VERTEX-70 spectrometer using KBr pellets ranging from  $400 \text{ cm}^{-1}$  to  $4000 \text{ cm}^{-1}$ . The TGA curves were recorded in the region of  $30\text{--}800 \text{ }^\circ\text{C}$  using a heating rate of  $10 \text{ }^\circ\text{C min}^{-1}$  in a flowing  $\text{N}_2$  atmosphere on a NETZSCH STA 449 F5 Jupiter thermal analyser. Photoluminescence emission spectra, photoluminescence excitation spectra and time-resolved emission spectra were obtained from an EDINBURGH FLS 980 fluorescence spectrophotometer equipped with a monochromated 325 W Xe-arc excitation source and a visible detector (Hamamatsu R928P). The Commission Internationale de L'Eclairage (CIE) 1931 chromaticity coordinates and CCT were calculated according to the international CIE standards.

### Synthesis of 1

$\text{SmCl}_3\cdot 6\text{H}_2\text{O}$  (0.228 g, 0.600 mmol) and benzoic acid (0.240 g, 0.200 mmol) were dissolved together under stirring in 30 mL of water, followed by the  $\text{K}_{14}[\text{P}_2\text{W}_{19}\text{O}_{69}(\text{H}_2\text{O})]\cdot 24\text{H}_2\text{O}$  precursor (2.120 g, 0.465 mmol). The mixed solution was continuously stirred to produce a clear liquid. Then, the pH value of the mixed solution was tuned to 4.5 by the addition of 3 M KOH solution. Subsequently, the resulting solution was heated to  $60 \text{ }^\circ\text{C}$  for 1.5 hours, then tetramethyl-ammonium chloride (TMACl) (0.110 g, 1.000 mmol) was added and stirred for another 20–30 minutes. The resulting solution was cooled to room temperature and filtered. The filtered solution was evaporated for about two weeks, and the block crystal was obtained. Yield: 24.6% (based on  $\text{SmCl}_3\cdot 6\text{H}_2\text{O}$ ). Selected IR ( $\text{KBr}$ ,  $\text{cm}^{-1}$ ): 3445 (br), 1632 (s), 1589 (m), 1523 (s), 1486 (s), 1420 (s), 1089 (s), 1046 (s), 945 (s), 890 (s), 825 (s) and 718 (m). Elemental analyses (%): Calcd, C, 6.55; H, 1.94; N, 1.20; Found, C, 6.78; H, 1.82; N, 1.27.

### X-ray crystallography

A suitable good-quality sample of **1** was sealed in a capillary tube, and then the crystallographic data was collected on a Bruker Apex II CCD diffractometer at room temperature using

**Table 2** Crystallographic data and structure refinement parameters for **1**

	<b>1</b>
Empirical formula	$\text{C}_{19}\text{H}_{67}\text{SmK}_2\text{N}_3\text{O}_{54}\text{PW}_{11}$
Formula weight	3483.49
Temperature/K	296.0
Crystal system	Triclinic
Space group	$P\bar{1}$
$a$ [ $\text{\AA}$ ]	12.9313 (9)
$b$ [ $\text{\AA}$ ]	13.4857 (9)
$c$ [ $\text{\AA}$ ]	20.2019 (14)
$\alpha$ [ $^\circ$ ]	83.0200 (10)
$\beta$ [ $^\circ$ ]	78.1820 (10)
$\gamma$ [ $^\circ$ ]	75.1760 (10)
$V$ [ $\text{\AA}^3$ ]	3324.6 (4)
$Z$	2
$\rho_{\text{calcd}}$ [ $\text{g cm}^{-3}$ ]	3.390
$\mu$ [ $\text{mm}^{-1}$ ]	20.059
$F(000)$	3010.0
Index ranges	$-15 \leq h \leq 15$ $-16 \leq k \leq 16$ $-19 \leq l \leq 24$
Reflections collected	17 377
Independent reflections	11 721 [ $R_{\text{int}} = 0.0368$ ]
data/restraints/parameters	11 721/57/424
Goodness-of-fit on $F^2$	1.002
$R_1, wR_2$ [ $I > 2\sigma(I)$ ]	0.0444, 0.1015
$R_1, wR_2$ [all data]	0.0650, 0.1121
Largest diff. peak/hole/ $e \text{ \AA}^{-3}$	2.93/−2.20

graphite-monochromated  $\text{MoK}\alpha$  radiation ( $\lambda = 0.71073 \text{ \AA}$ ). Empirical absorption corrections were taken on a multi-scan absorption correction. All these structures were solved by direct methods and refined by the full-matrix least squares on  $F^2$  using the SHELXL-2018/1 program package.<sup>18</sup> During the solving and refinement process, all heavy atoms were first located by the full matrix least-squares refinements on  $F^2$  and Fourier syntheses using the SHELXS-1997 program package, which were further refined anisotropically. Most lattice water molecules were located using a Fourier map, and the remaining lattice water molecules were determined by the TGA results. The hydrogen atoms from the organic groups were placed in calculated positions and refined using a riding model. All the hydrogen atoms on water molecules could not be precisely located from the electron density map. Crystallographic data and structural refinement for **1** (CCDC 1940262†) are listed in Table 2.

## Conflicts of interest

There are no conflicts to declare.

## Acknowledgements

This work was financially supported by the National Natural Science Foundation of China of China (21771053, 21771054, 21571050 and 21573056), Natural Science Foundation of Henan Province (132300410144 and 162300410015), Henan Province Science and Technology Attack Plan Project

(182102210237), and the Major Project of Science and Technology, Education Department of Henan Province (20A150010) and the 2019 Students Innovative Pilot Plan of Henan University (201910475076).

## Notes and references

- (a) P. Ma, F. Hu, J. Wang and J. Niu, *Coord. Chem. Rev.*, 2019, **378**, 281–309; (b) J.-W. Zhao, Y.-Z. Li, L.-J. Chen and G.-Y. Yang, *Chem. Commun.*, 2016, **52**, 4418–4445; (c) D. Li, P. Ma, J. Wang and J. Niu, *Coord. Chem. Rev.*, 2019, **392**, 49–80; (d) Y.-F. Song and R. Tsunashima, *Chem. Soc. Rev.*, 2012, **41**, 7384–7402; (e) O. Oms, A. Dolbecq and P. Mialane, *Chem. Soc. Rev.*, 2012, **41**, 7497–7536; (f) H. Wu, X. Meng, R. Wan, P. Ma, J. Wang and J. Niu, *Inorg. Chem. Commun.*, 2018, **95**, 154–157; (g) Y. Liu, M. Jin, L. Chen and J. Zhao, *Acta Crystallogr., Sect. C: Struct. Chem.*, 2018, **74**, 1202–1221.
- (a) Q. Han, W. Li, S. Wang, J. He and M. Li, *ChemCatChem*, 2017, **9**, 1801–1807; (b) Z. Shi, G. Niu, Q. Han, X. Shi and M. Li, *Mol. Catal.*, 2018, **10**, 10–18; (c) P. Ma, F. Hu, R. Wan, Y. Huo, D. Zhang, J. Niu and J. Wang, *J. Mater. Chem. C*, 2016, **4**, 5424–5433; (d) Y. Fang, C. Xing, S. Zhan, M. Zhao, M. Li and H. Liu, *J. Mater. Chem. B*, 2019, **7**, 1933–1944; (e) Q. Xu, Y. Niu, G. Wang, Y. Li, Y. Zhao, V. Singh, J. Niu and J. Wang, *Mol. Catal.*, 2018, **453**, 93–99; (f) H. Wu, M. Zhi, C. Chen, Y. Zhu, P. Ma, J. Wang and J. Niu, *Dalton Trans.*, 2019, **48**, 13850–13857.
- R. D. Peacock and T. J. R. Weakley, *J. Chem. Soc. A*, 1971, 1836–1839.
- (a) X. Ma, W. Yang, L. Chen and J. Zhao, *CrystEngComm*, 2015, **17**, 8175–8197; (b) Y. Liu, H. Li, C. Lu, P. Gong, X. Ma, L. Chen and J. Zhao, *Cryst. Growth Des.*, 2017, **17**, 3917–3928; (c) C. Boglio, G. Lemiere, B. Hasenknopf, S. Thorimbert, E. Lacote and M. Malacria, *Angew. Chem., Int. Ed.*, 2006, **45**, 3324–3327; (d) C. Boglio, G. Lenoble, C. Duhayon, B. Hasenknopf, R. Thouvenot, C. Zhang, R. C. Howell, B. P. Burton-Pye, L. C. Francesconi, E. Lacôte, S. Thorimbert, M. Malacria, C. Afonso and J.-C. Tabet, *Inorg. Chem.*, 2006, **45**, 1389–1398; (e) N. Belai, M. H. Dickman, M. T. Pope, R. Contant, B. Keita, I. Mbomekalle and L. Nadjo, *Inorg. Chem.*, 2005, **44**, 169–171; (f) P. Ma, R. Wan, Y. Si, F. Hu, Y. Wang, J. Niu and J. Wang, *Dalton Trans.*, 2015, **44**, 11514–11523.
- T. Yamase, in *Handbook on the Physics and Chemistry of Rare Earths*, Elsevier, 2009, vol. 39, pp. 297–356.
- (a) H. L. Li, Y. J. Liu, J. L. Liu, L. J. Chen, J. W. Zhao and G. Y. Yang, *Chem. – Eur. J.*, 2017, **23**, 2673–2689; (b) R. Ban, X. Sun, J. Wang, P. Ma, C. Zhang, J. Niu and J. Wang, *Dalton Trans.*, 2017, **46**, 5856–5863; (c) P. Ma, R. Wan, Y. Si, F. Hu, Y. Wang, J. Niu and J. Wang, *Dalton Trans.*, 2015, **44**, 11514–11523; (d) S. Chen, P. Ma, H. Luo, Y. Wang, J. Niu and J. Wang, *Chem. Commun.*, 2017, **53**, 3709–3712; (e) H. Wu, B. Yan, H. Li, V. Singh, P. Ma, J. Niu and J. Wang, *Inorg. Chem.*, 2018, **57**, 7665–7675.
- (a) M. Shang, C. Li and J. Lin, *Chem. Soc. Rev.*, 2014, **43**, 1372–1386; (b) P. Chen, Q. Li, S. Grindy and N. Holten Andersen, *J. Am. Chem. Soc.*, 2015, **137**, 11590–11593; (c) Y. Zhang, G. G. Li, D. L. Geng, M. M. Shang, C. Peng and J. Lin, *Inorg. Chem.*, 2012, **51**, 11655–11664.
- W. Zhao, C. Zou, L. Shi, J. Yu, G. Qian and C. Wu, *Dalton Trans.*, 2012, **41**, 10091–10096.
- (a) H. Ji, X. Li, D. Xu, Y. Zhou, L. Zhang, Z. Zuhra and S. Yang, *Inorg. Chem.*, 2017, **56**, 156–166; (b) H. Zhang, X. Li, L. Zhang, Y. Zhou, X. Ren and M. Liu, *J. Alloys Compd.*, 2018, **749**, 229–235.
- A. M. Kaczmarek, R. Van Deun and K. Van Hecke, *Dalton Trans.*, 2019, **48**, 8186–8192.
- (a) H. Wu, R. Wan, Y. Si, P. Ma, J. Wang and J. Niu, *Dalton Trans.*, 2018, **47**, 1958–1965; (b) H. Wu, M. Zhi, V. Singh, H. Li, P. Ma, J. Wang and J. Niu, *Dalton Trans.*, 2018, **47**, 13949–13956; (c) H. Wu, M. Zhi, H. Chen, V. Singh, P. Ma, J. Wang and J. Niu, *Spectrochim. Acta, Part A*, 2019, **223**, 117294.
- (a) *Rare earth coordination chemistry: fundamentals and applications*, ed. C.-H. Huang, John Wiley & Sons, 2010, p. 6; (b) B. R. Judd, *Phys. Rev.*, 1962, **127**, 750; (c) G. S. Ofelt, *J. Chem. Phys.*, 1962, **37**, 511; (d) D. William, J. Horrocks and R. S. Daniel, *J. Am. Chem. Soc.*, 1979, **101**, 334–340.
- (a) T. Yamase, *Chem. Rev.*, 1998, **98**, 307–325; (b) C. Zhang, R. Howell, D. McGregor, L. Bensaid, S. Rahyab, M. Nayshtut, S. Lekperic and L. Francesconi, *C. R. Chim.*, 2005, **8**, 1035–1044; (c) T. Yamase, T. Kobayashi, M. Sugeta and H. Naruke, *J. Phys. Chem. A*, 1997, **101**, 5046–5053.
- H. Wu, H. Chen, M. Fu, R. Li, P. Ma, J. Wang and J. Niu, *Dyes Pigm.*, 2019, **171**, 107696.
- (a) L. Bokatial and S. Rai, *J. Lumin.*, 2010, **130**, 1857–1862; (b) A. N. Meza-Rocha, A. Speghini, M. Bettinelli and U. Caldico, *J. Lumin.*, 2015, **167**, 305–309; (c) U. Caldico, A. Speghini, S. Berneschi, M. Bettinelli, M. Brenci, S. Pelli and G. C. Righini, *Opt. Mater.*, 2012, **34**, 1067–1071.
- (a) C. Ritchie, V. Baslon, E. G. Moore, C. Reber and C. Boskovic, *Inorg. Chem.*, 2012, **51**, 1142–1151; (b) C. Ritchie, E. G. Moore, M. Speldrich, P. Kögerler and C. Boskovic, *Angew. Chem., Int. Ed.*, 2010, **49**, 7702–7705.
- A. H. Ismail, B. S. Bassil, I. Römer, N. C. Redeker and U. Kortz, *Z. Naturforsch., B: J. Chem. Sci.*, 2010, **65**, 383–393.
- (a) G. M. Sheldrick, *Acta Crystallogr., Sect. C: Struct. Chem.*, 2015, **71**, 3–8; (b) A. L. Spek, *Acta Crystallogr., Sect. C: Struct. Chem.*, 2015, **71**, 9–18.